International Journal of Nanomedicine

Dovepress
open access to scientific and medical research

Open Access Full Text Article

ORIGINAL RESEARCH

Cu_3P/1-MT Nanocomposites Potentiated Photothermal-Immunotherapy

Jiawen He[1,2,*], Ruixiang Song[1,*], Fengfeng Xiao[2], Meng Wang[3], Liewei Wen[2]

[1]Key Laboratory of Biomedical Engineering of Hainan Province, School of Biomedical Engineering, Hainan University, Haikou, People's Republic of China; [2]Guangdong Provincial Key Laboratory of Tumor Interventional Diagnosis and Treatment, Zhuhai People's Hospital (Zhuhai Hospital Affiliated with Jinan University), Jinan University, Zhuhai, People's Republic of China; [3]Center for Biomedical Optics and Photonics (CBOP) & College of Physics and Optoelectronic Engineering, Key Laboratory of Optoelectronic Devices and Systems of Guangdong Province and Ministry of Education, Shenzhen University, Shenzhen, People's Republic of China

*These authors contributed equally to this work

Correspondence: Liewei Wen, Zhuhai People's Hospital, (Zhuhai Hospital Affiliated with Jinan University), Jinan University, Zhuhai, Guangdong, 519000, People's Republic of China, Tel +86-756-2158358, Fax +86-756-2157515, Email wenliewei@ext.jnu.edu.cn; wenner1989@163.com; Meng Wang, Center for Biomedical Optics and Photonics (CBOP) & College of Physics and Optoelectronic Engineering, Key Laboratory of Optoelectronic Devices and Systems of Guangdong Province and Ministry of Education, Shenzhen University, Shenzhen, People's Republic of China, Email wangmengst@szu.edu.cn

Purpose: Photothermal therapy (PTT) is a promising anticancer treatment that involves inducing thermal ablation and enhancing antitumor immune responses. However, it is difficult to completely eradicate tumor foci through thermal ablation alone. Additionally, the PTT elicited antitumor immune responses are often insufficient to prevent tumor recurrence or metastasis, due to the presence of an immunosuppressive microenvironment. Therefore, combining photothermal and immunotherapy is believed to be a more effective treatment approach as it can modulate the immune microenvironment and amplify the post-ablation immune response.

Methods: Herein, the indoleamine 2, 3-dioxygenase-1 inhibitors (1-MT) loaded copper (I) phosphide nanocomposites (Cu_3P/1-MT NPs) are prepared for PTT and immunotherapy. The thermal variations of the Cu_3P/1-MT NPs solution under different conditions were measured. The cellular cytotoxicity and immunogenic cell death (ICD) induction efficiency of Cu_3P/1-MT NPs were analyzed by cell counting kit-8 assay and flow cytometry in 4T1 cells. And the immune response and antitumor therapeutic efficacy of Cu_3P/1-MT NPs were evaluated in 4T1-tumor bearing mice.

Results: Even at low energy of laser irradiation, Cu_3P/1-MT NPs remarkably enhanced PTT efficacy and induced immunogenic tumor cell death. Particularly, the tumor-associated antigens (TAAs) could help promote the maturation of dendritic cells (DCs) and antigen presentation, which further activates infiltration of $CD8^+$ T cells through synergistically inhibiting the indoleamine 2, 3-dioxygenase-1. Additionally, Cu_3P/1-MT NPs decreased the suppressive immune cells such as regulatory T cells (Tregs) and M2 macrophages, indicating an immune suppression modulation effect.

Conclusion: Cu_3P/1-MT nanocomposites with excellent photothermal conversion efficiency and immunomodulatory properties were prepared. In addition to enhanced the PTT efficacy and induced immunogenic tumor cell death, it also modulated the immunosuppressive microenvironment. Thereby, this study is expected to offer a practical and convenient approach to amplify the antitumor therapeutic efficiency with photothermal-immunotherapy.

Keywords: copper (I) phosphide (Cu_3P), photothermal therapy, IDO-1 inhibitors, immunotherapy

Introduction

Photothermal therapy (PTT) is rapidly emerging as a highly effective and significant strategy for tumor therapy. Due to its high efficiency and non-invasive nature, it has been widely applied for treatment of malignant tumors such as melanoma, breast cancer, and pancreatic cancer.[1–5] Particularly, with the development of nanoparticles with better light absorption properties, it highly efficiently absorbs near-infrared (NIR) light and converts it into heat (>42 °C), thereby causing cell death.[6] PTT can well control the hyperthermia damage at the site of the tumor, owing to the elaborate and convenient adjustment of NIR light, which endows PTT with the characteristics of low invasiveness and high

Received: 25 March 2023
Accepted: 26 May 2023
Published: 7 June 2023

specificity.[7–9] Moreover, tumors are more susceptible to heat damage than normal cells, because of the unique biological characteristics such as the abnormal blood flow and reduced heat dissipating ability in solid tumors.[10] This specificity confers PTT with highly advantageous therapeutic properties, making it gradually become an alternative strategy for certain tumor therapy, especially those that are not suitable for traditional surgical treatment.[11–13] In addition, a growing number of studies have indicated that PTT can not only effectively ablate local tumor lesions, but also inhibit metastasis by activating anti-tumor immune effects.[14–16] In clinical trials, PTT showed significant therapeutic effects in 603 patients with metastatic liver from colorectal carcinoma and 500 patients with hepatocellular carcinoma, respectively.[15,17]

To improve the performance of PTT, researchers have employed nanoparticles with exceptional photothermal conversion efficiency, including noble metal nanostructures such as gold nanospheres, gold nanorods, and multifunctional gold nanoshells.[18–25] However, the price of noble metals restricts their widespread use. Copper materials, on the other hand, have garnered the interest of researchers due to their low cost, biocompatibility, biodegradability, and multifunctional properties.[26] Copper-based nanomaterials have shown great promise in PTT due to their exceptional light absorption properties in the NIR region, which is enabled by the local surface plasmon resonance (LSPR).[27] Copper-based nanomaterials, such as copper sulfide (CuS), copper selenide (CuSe), and copper (CuTe) nanomaterials are examples of copper-based nanomaterials with excellent NIR light-activated photothermal characteristics resulting from copper vacancy in the crystal lattice.[28–30] Optics and electronics have been extensively studied in copper (I) phosphide (Cu_3P) nanocomposites (NPs), which are among copper-based nanomaterials.[31,32] Cu_3P NPs, a p-type semiconductor, display remarkable LSPR absorption in the NIR region.[33] Recent studies have shown that Cu_3P NPs additionally exhibit tunable absorption in the mid-IR region and Cu vacancy regulated properties, which indicates that they have the potential to be used as a photothermal conversion medium for PTT.[33]

High levels of tumor cell death, exposure of tumor-associated antigens (TAAs), and release of damage-associated molecular patterns (DAMPs), resulting in immunogenic cell death (ICD), are caused by the intense heat produced by PTT.[34] This process recruits immune cells and induces immune responses.[35] Despite the efficacy of PTT in destroying local tumors, it is difficult to completely eradicate tumor foci.[36] Due to the immunosuppressive tumor microenvironment, the immune responses elicited by ICD-based PTT are insufficient to inhibit tumor recurrence and metastasis.[37] Combining PTT with immunotherapy can increase the therapeutic efficacy against both primary tumors and distant metastatic cancer cells.[38,39] This combination enhances the immune responses induced by ICD to track and eliminate tumor cells.[40,41] PTT and several immunosuppressants, such as checkpoint inhibitors, indoleamine 2,3-dioxygenase (IDO-1) inhibitors, immune adjuvants, CAR-T therapy, and cytokine therapy, have exhibited significant therapeutic effects to date.[42–46] IDO inhibitors, in particular, have received considerable attention.[47] IDO-1 catalyzes the oxidative catabolism of tryptophan (Trp) to kynurenine (Kyn) in order to inhibit the proliferation of $CD8^+$ T cells and induce intratumoral recruitment of regulatory T cells (Tregs), which impedes the ICD-induced immunoreaction and enables cancer progression.[48–50] Therefore, inhibiting IDO-1 can potently activate the ICD-mediated immune response and enhance antitumor efficacy. However, current IDO inhibitors such as Epacadostat and NLG919 have insufficient therapeutic effects due to their limited bioavailability and high lipophilicity.[51,52] Consequently, IDO inhibitor-loaded photothermal agents are anticipated to overcome these limitations of PTT or immunotherapy alone and enhance therapeutic efficacy by modulating the immune microenvironment.

In this study, Cu_3P nanoparticles are prepared to serve as photothermal agents owing to their ideal optical characteristics and biocompatibility. Then, the IDO inhibitor (1-MT) is loaded into the Cu_3P NPs to form a nanocomposite (Cu_3P/1-MT) for PTT and immunotherapy. Benefiting from the excellent photothermal properties, even under low energy of laser irradiation, Cu_3P/1-MT could remarkably enhance PTT efficacy. Meanwhile, it also induces the immunogenic cell death and triggers the release of TAAs, which will promote the dendritic cell (DC) maturation and antigen presentation. Furthermore, the immunosuppressive microenvironment could be comprehensively reprogrammed with the IDO-1 pathway blocker 1-MT, which allows the infiltration of $CD8^+$ T cells while inhibiting suppressive immune cells, such as Tregs and M2 macrophages at the tumor lesions (Figure 1). Therefore, the Cu_3P/1-MT nanocomposites are expected to provide an easily accessible, safe and efficient agent for synergistically improving the efficacy of PTT-immunotherapy.

Materials and Methods

Reagents

$CuCl_2 \cdot 2H_2O$, 1-Hexadecylamine (HDA), Trioctylphosphine oxide (TPOP), 2,7-dichlorofluorescein diacetate (DCFH-DA), 1-methyl tryptophan (1-MT), and 1-octadecene (ODE) were purchased from Sigma-Aldrich. Hyaluronic acid sodium (HA), cyclohexane, and ethanol were purchased from Aladdin Reagents. All chemicals were used as received without any additional purification unless otherwise stated.

Cells

The 4T1 breast cancer cells obtained from ATCC were grown in Gibco RPMI 1640 Medium supplemented with 10% fetal bovine serum (FBS; Gibco), 100 μg/mL penicillin (Gibco), and 100 μg/mL streptomycin (Gibco). The cells were routinely tested for the presence of Mycoplasma and maintained in a 37 °C humidified atmosphere containing 5% CO_2. Using standard techniques, bone marrow-derived macrophages and dendritic cells (BMDMs & BMDCs) were isolated from BALB/c mice. The mice were euthanized, and bone marrow cells were extracted from their leg bones. The extracted cells were then maintained in an RPMI medium supplemented with 10% FBS. Monocytes were differentiated for seven days with GM-CSF and IL-4 in order to collect BMDMs.

Xenograft Tumor Model

Female BALB/c mice (6–8 weeks) were purchased from Guangdong Medical Laboratory Animal Center (Guangzhou, China). The 4T1 cells (5×10^5) were subcutaneously injected into the back of BALB/c mice. Once the tumor volume reached between 100 and 150 mm^3, the mice were randomly assigned to our experiments. All the experiments were performed under protocols approved by the Animal Research Ethics Committee of Hainan university (ethics approval number: HNUAUCC-2021-00025).

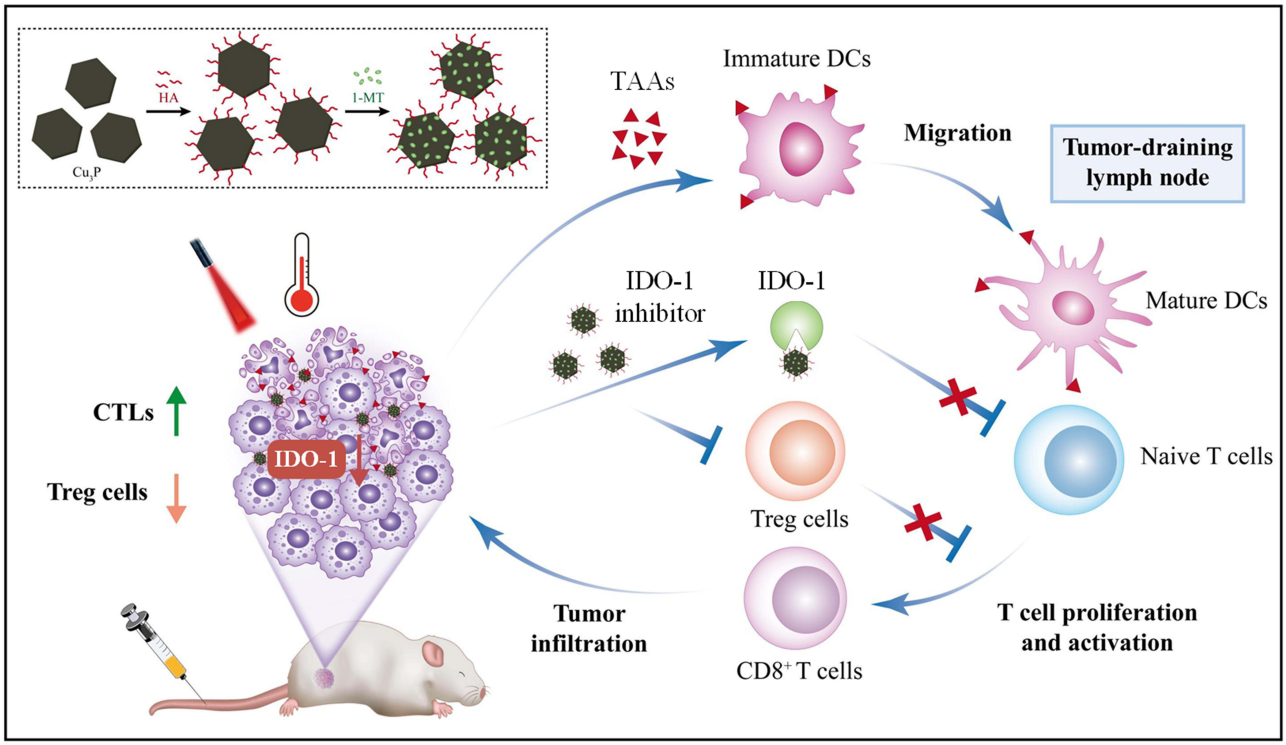

Figure 1 Schematic illustration of PTT-immunotherapy potentiated by Cu_3P/1-MT nanocomposites.

Synthesis of Cu_3P

In accordance with a standard method for synthesizing Cu_3P NPs, the following were added to a 50 mL three-neck flask: 0.5 mmol $CuCl_2{\cdot}2H_2O$, 1.209 g of HAD, 1.551 g of TPOP, and 12 mL of ODE. Under a N_2 atmosphere, the solution was dehydrated by heating it for 30 minutes at 150 °C. Subsequently, the temperature was raised to 300 °C for 1.5 hours in an atmosphere of N_2 before being cooled to 25 °C. The resultant NPs were combined with ethanol to create nanoparticles, then centrifuged at 8000 rpm for 5 minutes and washed three times with cyclohexane and ethanol.

Synthesis of HA-Capped Cu_3P/1-MT

Cu_3P NPs were dispersed in an ethanol solution of HA and sonicated for one hour. The resulting mixture was stirred for 12 hours before being centrifuged at 10,000 rpm for 5 minutes to collect the HA-capped Cu_3P NPs. Next, they were washed three times with water before being redistributed in PBS. Approximately 8 mg 1-MT was added to the HA-capped Cu_3P NPs solution (20 mL, 1 mg/mL in PBS for 1-MT loading). To collect Cu_3P/1-MT, the mixture was stirred overnight at 25 °C and centrifuged at 13,000 rpm for 10 minutes. Using fluorescence spectrophotometry with an excitation wavelength of 285 nm and an emission wavelength of 355 nm, the amount of 1-MT that was loaded was determined. The following equation was used to determine the loading efficiency of 1-MT:

$$\text{loading capacity of 1 - MT (\%)} = \frac{(\text{weight of 1 - MT}) - (\text{weight of unloaded 1 - MT})}{(\text{weight of 1 - MT})} \times 100\%$$

Characterization of NPs

Powder X-ray diffraction patterns for samples were acquired using an X-ray diffractometer (MiniFlex2, Rigaku, Japan) with Cu Kα1 radiation (λ = 0.154187 nm). Additionally, a JEOL-2010 transmission electron microscope (TEM, JEOL, Japan) was utilized to carry out the TEM measurements. Moreover, a UV-vis-NIR spectrophotometer (Cary 50 Bio, USA) was utilized to determine the amounts of loaded 1-MT. In addition, the FTIR spectra were obtained by compressing thin films composed of samples and potassium bromide (KBr) powder. Subsequently, a Fourier Transform Infrared spectrometer (FTIR, Frontier, PerkinElmer, USA) was used for acquiring the FTIR spectra of the samples.

In vitro Phototoxicity of Cu_3P/1-MT NPs

The phototoxicity of Cu_3P/1-MT NPs was evaluated using the CCK-8 assay. 4T1 cells were seeded at a density of 5×10^3 cells per well in a 96-well plate and incubated for 12 hours. Subsequently, the cells were exposed to Cu_3P/1-MT NPs at varying concentrations. The cells were then exposed to 808 nm laser irradiation with an intensity of 0.8 W/cm^2 for 5 minutes, followed by 24 hours of incubation for CCK-8 cell viability assay.

Cell Staining Assays

For the cell death assay, the cells were stained with calcein acetoxymethyl ester (calcein-AM)/PI, which were then detected using a fluorescence microscope (MD43-N, Mshot, Guangzhou, China). To indicate calreticulin (CRT) expression, the cells were stained with anti-rabbit CRT polyclonal antibody (Immunoway, Beijing, China) and Alexa Fluor Plus 488-Goat anti-rabbit IgG (Invitrogen) at 1 hour after laser irradiation.

Maturation of DCs

To conduct DC stimulation experiments in vitro, each 1×10^6 DCs were placed in 12-well plates. After an incubation period of approximately 24 hours, the cells were co-incubated with tumor cells that had been treated with Cu_3P/1-MT NPs, PBS + L, or Cu_3P/1-MT NPs + L. The BMDCs were then stained with anti-CD86-PE antibodies and analyzed with a Stratedigm S1200Ex flow cytometer (Stratedigm, USA).

Anticancer Efficacy in vivo

The tumor-bearing mice were randomly divided into four groups of five mice each: the PBS group, the Cu_3P/1-MT NPs group, the Cu_3P NPs + L group, and the Cu_3P/1-MT NPs + L group. Following intravenous administration of either PBS

or related NPs, PTT was performed using an 808 nm laser for 10 minutes with a power density of 0.8 W/cm^2. The optical fiber used to provide uniform light distribution on the treatment surface was manufactured by Pioneer Optics of Bloomfield, Connecticut. The temperature of the surface of the tumor was measured using an infrared thermal camera E80 (FLIR, Boston, USA). Using a digital caliper, tumor size was measured every two days, and the ellipsoidal formula $V = (\text{width})^2 \times \text{length} \times 2^{-1}$ was used to calculate the tumor volume. When tumors reached a maximum size of 2.0 cm in any dimension or when ulcerations appeared, the mice were euthanized.

Flow Cytometry

The tumor tissues were harvested, minced, and then digested at 37 °C for 20–30 minutes with Collagenase IV (1 mg/mL) and DNase I (20 μg/mL) in RPMI. In addition, the spleen was gathered, ground, and treated with ACK lysis buffer to eliminate red blood cells. To obtain a single-cell solution, the remaining cells were filtered and washed in PBS. To minimize non-specific bindings to Fc receptors, anti-CD16/32 (clone 93; eBioscience, USA) was used. The cells were then stained with the following antitumor fluorescent antibodies in order to evaluate active T cells: Live/Dead-Zombie 405, CD45-eFluor 450, CD3-APC-eFluor 780, CD8a-FITC, CD4-PE-CY7, CD25-APC, and Foxp3-PE. Cells were stained with Live/Dead-Zombie 405, CD45-eFluor 450, CD11b-PE, F4/80-APC, and CD206-FITC in order to evaluate tumor-associated macrophages (TAM). Stratedigm S1200Ex flow cytometer (Stratedigm, USA) and FlowJo software were used to analyze the procedure.

Statistical Analysis

Statistical comparisons were carried out using SPSS 23.0 (IBM Corp., Armonk, NY, USA) and described as mean ± standard deviation. Figures were performed using GraphPad Prism 8.1 (GraphPad Software, Inc., La Jolla, CA, USA). The Shapiro–Wilk test was used for normal distribution. The data were normally distributed. The Student's *t*-test was used for comparing two groups. The difference between multiple groups was analyzed by one-way analysis of variance followed by Tukey's test. The difference was considered statistically significant at $P < 0.05$.

Results and Discussion

Synthesis and Characterization of Cu_3P/1-MT

Cu_3P NPs were obtained as described previously.[53] The morphology of the resulting NPs was confirmed by TEM, as depicted in Figure 2a. The images displayed the platelet-like hexagonal shape of Cu_3P NPs, with a size of approximately 97.9 nm (Figure 2b). The previous study demonstrates that platelet-like hexagonal NPs, also known as nanoplatelets, are more cellular uptake-friendly than nanorods.[54] X-ray diffraction (XRD) and X-ray photoelectron spectroscopy (XPS) were used to characterize Cu_3P NPs, as shown in Figure 2c and d. The XRD pattern of Cu_3P NPs was in accordance with the hexagonal phase of Cu_3P. There are several diffraction peaks at 36.1°, 39.3°, 41.7°, 45.1°, and 46.5°, corresponding to (112), (202), (211), (300), and (113) planes of hexagonal Cu_3P, respectively.[33,55] Two prominent peaks in the XPS spectrum of Cu 2p at 932.2 eV (Cu 2p3/2) and 952.1 eV (Cu 2p1/2) indicate that Cu is present in the form of Cu 2p (I). Figure 2e depicts an optical absorption of these platelets in the NIR region, supporting their viability as a candidate photothermal agent. The outer surface of Cu_3P NPs was coated with hyaluronic acid to improve their dispersibility and hydrophilicity. The 1-MT was then capped to Cu_3P@HA to produce Cu_3P/1-MT. Figure 2f displays the Fourier transform infrared (FTIR) spectra of Cu_3P, Cu_3P@HA, and Cu_3P/1-MT components. After HA was capped, the peak around the 1203 cm^{-1} fingerprint region corresponds to the -C-O-C- stretching vibration, the band at 2903 cm^{-1} corresponds to the characteristic vibrations of C-H stretching of HA, and the broad band at 3411 cm^{-1} indicates the O-H stretching of HA.[53] In addition, the stretching vibrations of benzene and heteroaromatic rings at 1540 cm^{-1} and 1400 cm^{-1} were observed in Cu_3P/1-MT, confirming the successful loading of Cu_3P/1-MT. The amount of loaded 1-MT was quantified using a fluorescence spectrophotometer, and the final drug load rate was determined to be 68%.

The photothermal properties of Cu_3P/1-MT NPs were further investigated by laser-induced temperature monitoring. Different concentrations (0.25, 0.5, 1, and 1.5 mg/mL) of Cu_3P/1-MT NPs were exposed to 808 nm NIR light (0.8 W/cm^2) for 8 minutes, and temperature changes were monitored until the 14th minute. As depicted in Figure 2g, the temperature of a solution of Cu_3P/1-MT NPs increased with increasing irradiation intensity and concentration. Within an 8-minute timeframe, laser irradiation at a power density of 0.8 W/cm² can elevate the temperature of 1.5 mg/mL Cu_3P/1-MT NPs solution by nearly 30 °C (Figure 2h).

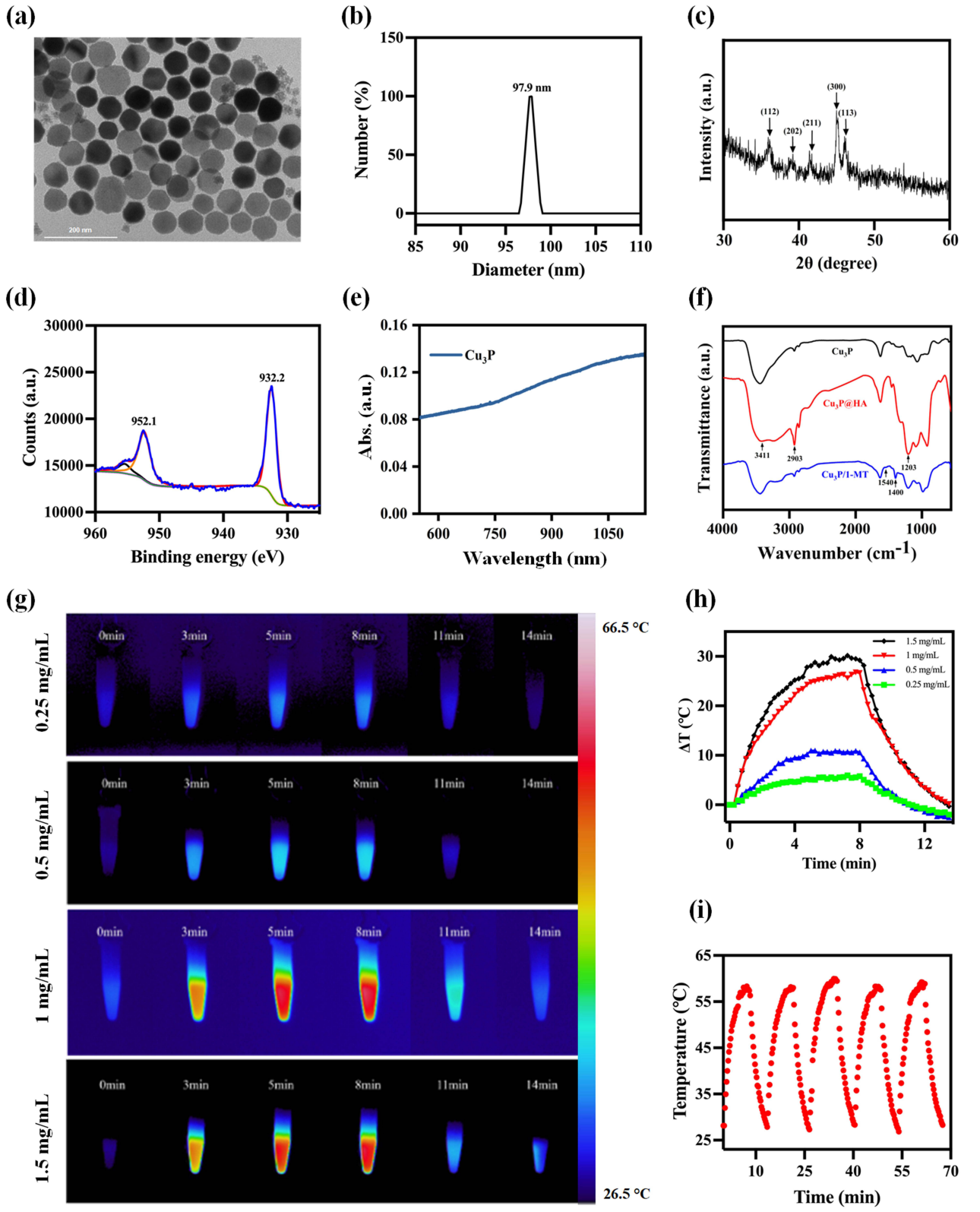

Figure 2 Synthesis and characterization of Cu_3P/1-MT NPs. (**a**) TEM image of Cu_3P NPs. Scale bar = 200 nm. (**b**) Size distribution of Cu_3P NPs. (**c**) XRD of Cu_3P NPs. (**d**) XPS spectra of Cu_3P NPs. (**e**) Vis–NIR absorbance spectrum of Cu_3P NPs. (**f**) FTIR spectra of Cu_3P, Cu_3P@HA, Cu_3P/1-MT NPs. (**g**) Near-infrared thermal images for Cu_3P/1-MT NPs solution of different concentrations (0.25, 0.5, 1 and 1.5 mg/mL) under 808 nm laser irradiation at 0.8 W/cm^2. (**h**) Infrared thermal imaging-based temperature elevation records. (**i**) Temperature curves of Cu_3P/1-MT NPs during five times "on/off" irradiation with 808 nm laser at 0.8 W/cm^2.

The photothermal stability of Cu_3P/1-MT NPs power density was set as 0.8w/cm^2, the laser irradiation was cycled five times, the interval time for per cycle is 2 minutes and no discernible degradation was observed (Figure 2i). These results demonstrated that the Cu_3P/1-MT NPs could be an effective photothermal agent for PTT.

Cu_3P/1-MT Enhanced PTT in vitro

To examine the biocompatibility of Cu_3P/1-MT NPs, the cytotoxicity of 4T1 tumor cells treated with Cu_3P/1-MT NPs (0, 25, 50, 100, and 200 μg/mL) was examined using the standard cell counting kit-8 (CCK-8) assay (Figure 3a). 4T1 cells were incubated with Cu_3P/1-MT NPs for 12 hours, followed with or without laser irradiation. More than 95% of 4T1 cells exposed to 200 μg/mL of Cu_3P/1-MT NPs survived in the absence of laser irradiation, indicating excellent biocompatibility. Conversely, with 50 μg/mL of Cu_3P/1-MT NPs, nearly 50% of laser-irradiated cells were killed, and the cytotoxicity was concentration-dependent. This provided support for the viability of Cu_3P/1-MT NPs in PTT. Afterward, 4T1 cells treated with 200 μg/mL Cu_3P/1-MT NPs were examined for the presence of live (calcein AM-stained, green) and dead (PI-stained, red) cells. Overall, the results indicated that Cu_3P/1-MT might have enormous potential for achieving photothermal ablation of cancer cells.

By exposing DAMPs on the cell surface, PTT has been shown to induce synergistic ICD.[56] These DAMPs, such as CRT, HMGB1, and ATP, could act as "eat-me" signals to activate DCs.[57,58] Cu_3P NPs-based PTT induced CRT exposure was, therefore, tested as an indicator of ICD induction. Flow cytometry demonstrated that laser irradiation of Cu_3P/1-MT-treated cells resulted in a 7-fold higher CRT level than in the Cu_3P/1-MT group (Figure 3b). Therefore, Cu_3P/1-MT-based PTT exhibited exceptional ICD-induced efficiency. DCs are the most formidable antigen-presenting cells. DCs presented antigen potently in order to stimulate naive T cell activation and proliferation.[59] The levels of $CD80^+$ and $CD86^+$ were utilized to denote DCs' maturation.[60] To evaluate the antitumor immune response, the maturation of DCs stimulated by treated tumor cells with PBS, Cu_3P/1-MT, or Cu_3P/1-MT + NIR laser was evaluated using flow cytometry (Figure 3c). In the group of 4T1 cells treated with Cu_3P/1-MT, the expression of $CD86^+$ in DCs was found to be only 1.3% higher compared to the 4T1 cells treated with PBS group. This suggests that Cu_3P/1-MT treatment without PTT has limited capacity to induce DC maturation. When 4T1 cells were treated with Cu_3P/1-MT and NIR laser irradiation, a 3.1-fold increase in $CD86^+$ expression was observed compared to Cu_3P/1-MT alone, demonstrating the critical role of laser irradiation in Cu_3P/1-MT NPs-induced DCs maturation. The findings suggested that Cu_3P/1-MT with laser irradiation can significantly promote DC maturation by inducing TAAs and inhibiting the IDO pathway with 1-MT. Overall, these in vitro results confirmed that Cu_3P/1-MT plus laser-induced ICD, with enhanced maturation of DCs and mass 4T1 cell death.

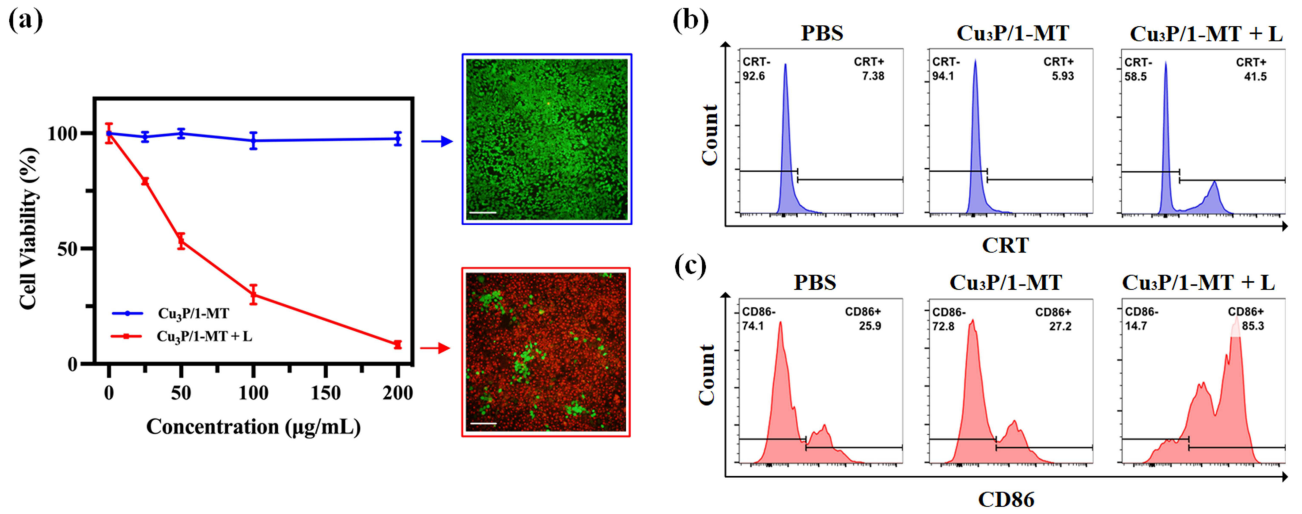

Figure 3 Cu_3P/1-MT NPs enhanced PTT in vitro. (**a**) Cell viability and fluorescence images with or without laser irradiation (808 nm, 0.8 W/cm^2) for different concentrations of Cu_3P/1-MT NPs (n = 4). Scale bar = 100 μm. (**b**) Flow cytometry analysis of CRT in differently treated with 4T1 cells. (**c**) Flow cytometry indicated CD86 positive DCs induced by Cu_3P/1-MT NPs treated 4T1 cells.

In vivo PTT Efficacy

To assess the photothermal effects of Cu_3P/1-MT NPs in vivo, we conducted experiments on 4T1 tumor-bearing mice (Figure 4a). An 808 nm laser was used to measure the photothermal effect of Cu_3P/1-MT NPs. Accordingly, in vivo photothermal imaging was performed on tumor-bearing mice administered either PBS or Cu_3P/1-MT NPs for 24 hours. As measured in vivo with an infrared thermal camera, laser irradiation of mice treated with Cu_3P/1-MT NPs caused a rapid 25 °C-temperature increase on the tumor surface. Compared to the Cu_3P/1-MT NPs group, the increase in temperature in the tumor regions of the PBS + NIR laser group was only approximately 10 °C, indicating a lower effect. The results support the high absorption and photothermal conversion efficiency of Cu_3P/1-MT nanoparticles at 808 nm in vivo.

To examine the killing effect of Cu_3P/1-MT NPs in vivo, 4T1 tumor-bearing mice were randomly assigned to PBS + L, Cu_3P/1-MT NPs, and Cu_3P/1-MT NPs + L treatment groups. The harvested tumor section was stained with terminal deoxynucleotidyl transferase dUTP nick end labeling (TUNEL) and hematoxylin and eosin (H&E) seven days after laser treatment (Figure 4b). Compared to the PBS + L or Cu_3P/1-MT NPs group, the Cu_3P/1-MT NPs + NIR laser group induced a significant amount of apoptosis in the tumors, as shown by TUNEL staining. Similar trends were observed in the H&E staining, with the Cu_3P/1-MT NPs + NIR laser group exhibiting significantly more cancer cells with deformed nuclei (karyopyknosis, karyorrhexis, and karyolysis) than the other groups. TUNEL and H&E tests revealed that synergistic treatment with Cu_3P/1-MT NPs + NIR laser was more effective than immunotherapy alone (Cu_3P/1-MT NPs group).

Cu_3P/1-MT-Induced Immune Response

The DAMPs and antigens released by dying tumor cells after PTT can be transported to the spleen, thereby promoting DC recruitment and maturation, which results in a robust immune response from the host.[61] $CD8^+$ cytotoxic T lymphocytes and $CD4^+$ helper T lymphocytes play a vital role in this systemic host immune response. Compared to PBS + L group, increased $CD8^+$ T infiltration in the spleen was observed with the treatment of Cu_3P + L (1.4-fold) and Cu_3P/1-MT +L (1.6-fold), demonstrated in Figure 5a. $CD4^+$ T cells in the spleen were increased in Cu_3P/1-MT + L group higher than in any other group (Figure 5b). The Cu_3P + L and Cu_3P/1-MT +L groups had proportions of $CD8^+$ T cells in the primary tumor that was 1.6- and 2.2-fold greater than the PBS + L group, respectively (Figure 5c). As shown in Figure 5d, the Cu_3P/1-MT + L group had a 1.4-fold increase in $CD4^+$ T cells at tumor sites compared to the PBS + L group. These results indicated that the synergistic combination of Cu_3P/1-MT NPs and NIR laser could increase the infiltration of T cells systemically. Previous research also supported the inhibition of Treg cells by IDO.[48] We further explored the population of Treg cells in the tumors post-treatment by flow cytometry (gated on $CD4^+$ $CD25^+$ $Foxp3^+$ T cells, Figure 5e). The Treg population in tumors decreased from ≈29% to ≈25% in Cu_3P/1-MT NPs treated mice. In mice synergistically treated with Cu_3P/1-MT +L, the population of Treg cells decreased to ≈20% (Figure 5f). To investigate further whether immunosuppression in the tumor microenvironment had been reversed in tumor-bearing mice, alternatively

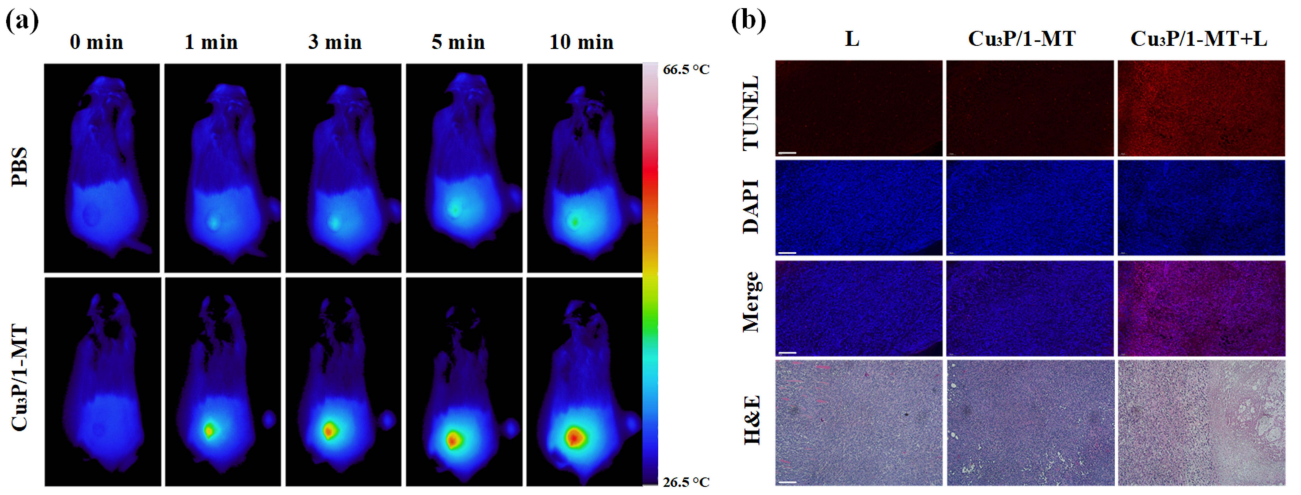

Figure 4 In vivo PTT efficacy. (**a**) Infrared thermal images of 4T1 tumor-bearing mice under Cu_3P/1-MT NPs and laser irradiation. (**b**) Representative TUNEL and H&E staining images for the primary tumors. Scale bar = 200 μm.

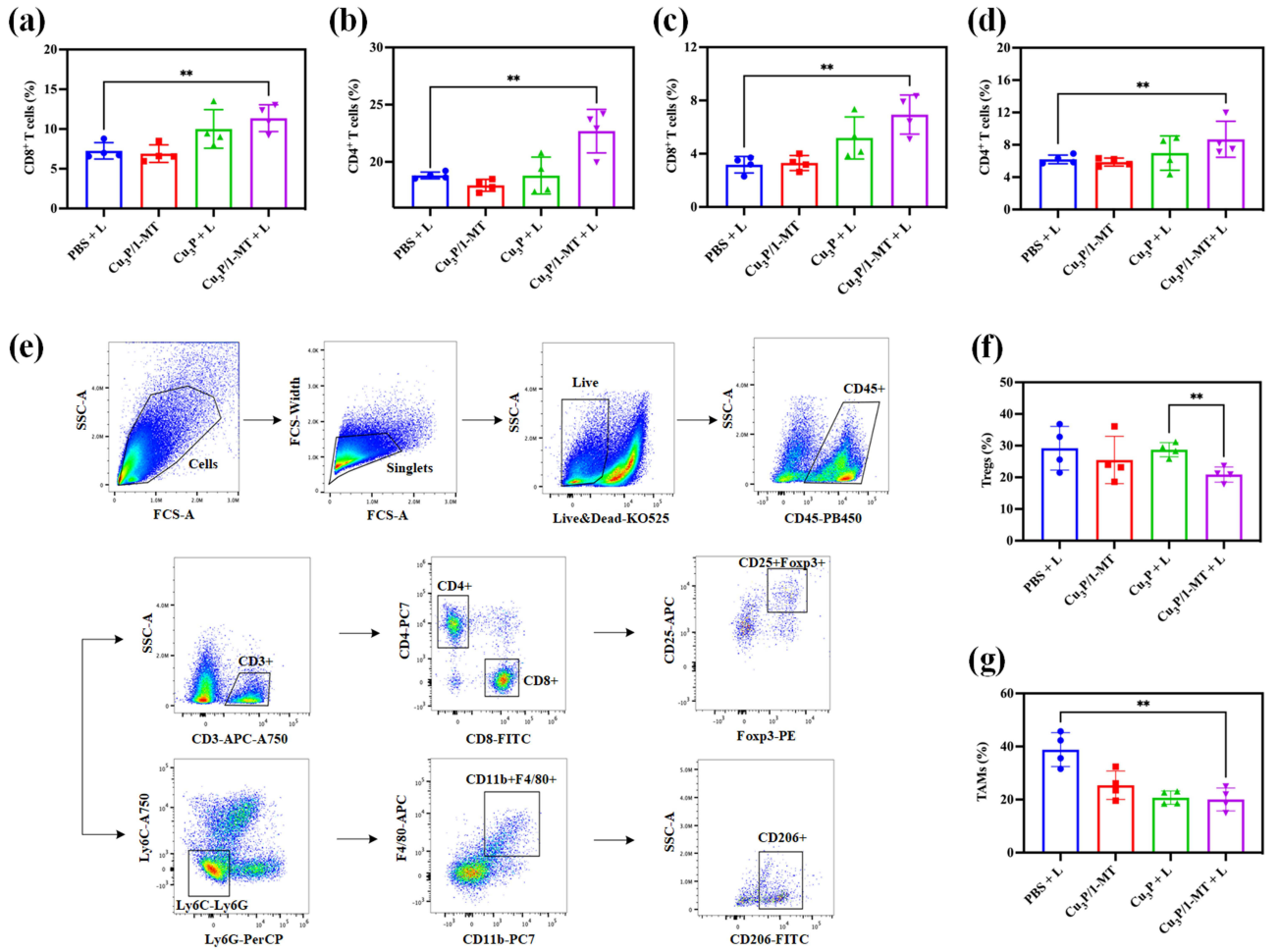

Figure 5 Cu_3P/1-MT NPs-induced immune response. Flow cytometry analyses of spleen $CD8^+$ (**a**) and $CD4^+$ (**b**) T cell subsets (n = 4, **P < 0.01). Intratumoral infiltration of $CD8^+$ (**c**) and $CD4^+$ (**d**) T cells in the primary tumor (n = 4, **P < 0.01). (**e**) Gating strategy showing the analysis of Treg cells and TAMs subsets from mouse tumors. (**f**) The level of tumor-infiltrating Treg cells was quantified by gating for $CD4^+CD25^+Foxp3^+$ cells (n = 4, **P < 0.01). (**g**) The level of tumor-infiltrating TAMs was quantified by gating for $CD11b^+F4/80^+CD206^+$ cells (n = 4, **P < 0.01).

Abbreviations: n.s., no significant difference.

activated myeloid (M2) cells (identified by flow cytometry, gated on $CD11b^+$ $F4/80^+$ $CD206^+$ Myeloid-derived suppressor cells, Figure 5e) were isolated from the primary tumor. The decrease of M2 macrophage was found in Cu_3P/1-MT, Cu_3P + L, and Cu_3P/1-MT +L groups (Figure 5g). Cu_3P/1-MT NPs decreased the proportion of M2 macrophages because 1-MT inhibited the recruitment and phagocytic function of macrophages and stimulated the polarization of macrophages towards the M1 state.[62] The reduction of M2 macrophages in the Cu_3P NPs-based PTT group revealed the transformation of a "cold tumor" into a "hot tumor". Taken together, these findings demonstrated that combining PTT with an IDO-1 inhibitor could effectively reverse the immunosuppressive microenvironment and enhance the post-ablation immune response, which explains its superior efficacy against tumors. Future research is warranted on the immune system-regulatory effect of photothermal agents with multiple functions.

Antitumor Effect and Side Effects

In light of the promising in vitro therapeutic effect of Cu_3P/1-MT NPs, the therapeutic efficacy of this system was evaluated in mice bearing the 4T1 tumor. When the volume of the tumors reached 100 mm^3, the mice received intravenous injections of the corresponding drugs. The mice were exposed to the 808 nm NIR laser for 10 minutes at a power density of 0.8 W/cm^2 for laser irradiation. The volumetric changes of a tumor are a direct indicator of therapeutic efficacy. Increasing tumor volume was observed in the PBS+NIR and Cu_3P/1-MT groups (Figure 6a). In contrast, the tumor in the laser irradiation co-treated mice (Cu_3P +L and Cu_3P/1-MT+L groups) seemed completely eliminated on day 25. Compared to the Cu_3P + L group, mice in the Cu_3P/

1-MT + L group had significantly longer survival times (Figure 6b). It is possible that the combination of PTT and IDO inhibitor (1-MT) could stimulate the body's natural long-term immunity, prevent tumor recurrence, and ultimately increase the individual survival rate. Throughout the 34-day therapeutic period, there were no measurable variations in the mice's body weights

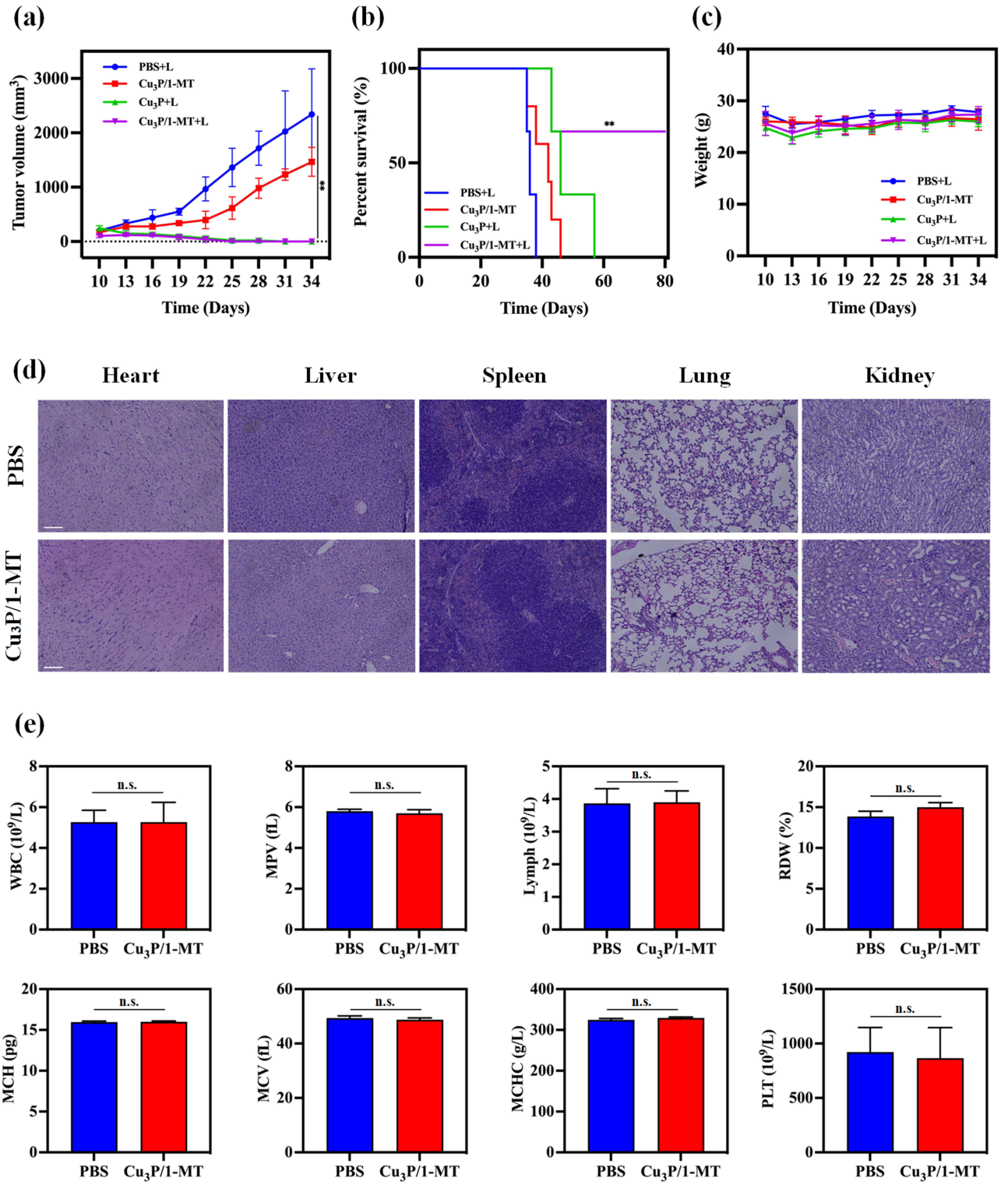

Figure 6 Antitumor effect and side effects. (**a**) Tumor growth curves of the primary tumor from treated mice (n = 5, **P < 0.01). (**b**) Survival percentage of mice after modeling (n=5, **P < 0.01). (**c**) Body weight changes of mice under treatment (n = 5). (**d**) Histopathological of main organs and (**e**) Hematological analysis evaluated of systemic toxicity. Scale bar = 200 μm.

Abbreviations: n.s., no significant difference.

(Figure 6c). No obvious damage was observed in the major organs (heart, liver, spleen, lung, and kidney) of mice treated with or without Cu_3P/1-MT NPs (Figure 6d), as determined by H&E staining. Body weight and H&E staining in the treated mice further demonstrated the biosecurity of our therapeutic approach. Blood samples were obtained from the mice to conduct hematological analysis. The analysis of standard hematology markers revealed no statistically significant differences among the various groups (Figure 6e). These findings indicate that the administration of Cu_3P/1-MT NPs and the therapeutic procedure did not result in noticeable infection or inflammation in the mice.

Conclusion

In this study, the IDO-1 pathway inhibitor 1-MT was utilized to develop an NP-containing NIR photothermal agent (Cu_3P/1-MT NPs) so that photothermal therapy and immunotherapy could be implemented synergistically to enhance therapeutic efficacy. In vitro and in vivo, the post-ablation immune response was amplified when treated with Cu_3P NPs and laser irritation. Specifically, Cu_3P/1-MT NPs significantly enhanced the maturation of DCs and immune cell infiltration at tumor sites while alleviating immunosuppression. Our research suggests a promising cancer treatment strategy to inhibit the growth of primary tumors and prolong individual survival, which will pave the way for the future application of potentiating PTT against various types of solid tumors.

Acknowledgments

This research was funded by Hainan Province Key Area R&D Program (ZDYF2021SHFZ094). The Guangdong Basic and Applied Basic Research Foundation (2021A1515011703, 2022A1515220167, 2021B1212040004).

Disclosure

The authors report no conflicts of interest in this work.

References

1. Liu S, He J, Song R, et al. Fe_2P nanorods based photothermal therapy combined with immune checkpoint inhibitors for pancreatic cancer. *Nanophotonics*. 2021;10(12):3267–3278. doi:10.1515/nanoph-2021-0196
2. Wu J, Wang S, Liu S, et al. Immunoadjuvant nanoparticles as trojan horses for enhanced photo-immunotherapy in the treatment of triple-negative breast cancer. *Front Pharmacol*. 2022;13:883428. doi:10.3389/fphar.2022.883428
3. Naylor MF, Zhou F, Geister BV, et al. Treatment of advanced melanoma with laser immunotherapy and ipilimumab. *J Biophotonics*. 2017;10(5):618–622. doi:10.1002/jbio.201600271
4. Wang W, Chen C, Ying Y, et al. Smart PdH@MnO_2 yolk–shell nanostructures for spatiotemporally synchronous targeted hydrogen delivery and oxygen-elevated phototherapy of melanoma. *ACS Nano*. 2022;16(4):5597–5614. doi:10.1021/acsnano.1c10450
5. Wang Z, Zhan M, Li W, et al. Photoacoustic cavitation-ignited reactive oxygen species to amplify peroxynitrite burst by photosensitization-free polymeric nanocapsules. *Angew Chem Int Ed Engl*. 2021;60(9):4720–4731. doi:10.1002/anie.202013301
6. Lv Z, He S, Wang Y, et al. Noble metal nanomaterials for NIR-triggered photothermal therapy in cancer. *Adv Healthc Mater*. 2021;10(6):e2001806. doi:10.1002/adhm.202001806
7. Zou L, Wang H, He B, et al. Current approaches of photothermal therapy in treating cancer metastasis with nanotherapeutics. *Theranostics*. 2016;6(6):762–772. doi:10.7150/thno.14988
8. Alamdari SG, Amini M, Jalilzadeh N, et al. Recent advances in nanoparticle-based photothermal therapy for breast cancer. *J Control Release*. 2022;349:269–303. doi:10.1016/j.jconrel.2022.06.050
9. Cai Z, Fu Y, Qiu Z, et al. Multitarget reaction programmable automatic diagnosis and treatment logic device. *ACS Nano*. 2021;15(12):19150–19164. doi:10.1021/acsnano.1c07307
10. Wen L, Liu H, Hu C, et al. Thermoacoustic imaging-guided thermo-chemotherapy for hepatocellular carcinoma sensitized by a microwave-responsive nitric oxide nanogenerator. *ACS Appl Mater Interfaces*. 2023;15(8):10477–10491. doi:10.1021/acsami.2c22523
11. Dewey WC, Hopwood LE, Sapareto SA, et al. Cellular responses to combinations of hyperthermia and radiation. *Radiology*. 1977;123(2):463–474. doi:10.1148/123.2.463
12. Nikfarjam M, Muralidharan V, Christophi C. Mechanisms of focal heat destruction of liver tumors. *J Surg Res*. 2005;127(2):208–223. doi:10.1016/j.jss.2005.02.009
13. Ni W, Li Y, Liang L, et al. Tumor microenvironment-responsive nanodrug for clear-cell renal cell carcinoma therapy via triggering waterfall-like cascade ferroptosis. 2021.
14. Hu Y, Chi C, Wang S, et al. A comparative study of clinical intervention and interventional photothermal therapy for pancreatic cancer. *Adv Mater*. 2017;29(33):1700448. doi:10.1002/adma.201700448
15. Pacella CM, Bizzarri G, Magnolfi F, et al. Laser thermal ablation in the treatment of small hepatocellular carcinoma: results in 74 patients. *Radiology*. 2001;221(3):712–720. doi:10.1148/radiol.2213001501
16. Zhang X, Ong'achwa Machuki J, Pan W, et al. Carbon nitride hollow theranostic nanoregulators executing laser-activatable water splitting for enhanced ultrasound/fluorescence imaging and cooperative phototherapy. *ACS Nano*. 2020;14(4):4045–4060. doi:10.1021/acsnano.9b08737

17. Arienti V, Pretolani S, Pacella CM, et al. Complications of laser ablation for hepatocellular carcinoma: a multicenter study. *Radiology*. 2008;246(3):947–955. doi:10.1148/radiol.2463070390
18. Liu H, Chen D, Li L, et al. Multifunctional gold nanoshells on silica nanorattles: a platform for the combination of photothermal therapy and chemotherapy with low systemic toxicity. *Angew Chem Int Ed Engl*. 2011;50(4):891–895. doi:10.1002/anie.201002820
19. Liu H, Liu T, Wu X, et al. Targeting gold nanoshells on silica nanorattles: a drug cocktail to fight breast tumors via a single irradiation with near-infrared laser light. *Adv Mater*. 2012;24(6):755–761. doi:10.1002/adma.201103343
20. Xu P, Liang F. Nanomaterial-based tumor photothermal immunotherapy. *Int J Nanomedicine*. 2020;15:9159–9180. doi:10.2147/IJN.S249252
21. Qu X, Yao C, Wang J, et al. Anti-CD30-targeted gold nanoparticles for photothermal therapy of L-428 Hodgkin's cell. *Int J Nanomedicine*. 2012;7:6095–6103. doi:10.2147/IJN.S37212
22. Qin L, Niu D, Jiang Y, et al. Confined growth of multiple gold nanorices in dual-mesoporous silica nanospheres for improved computed tomography imaging and photothermal therapy. *Int J Nanomedicine*. 2019;14:1519–1532. doi:10.2147/IJN.S184192
23. Zhou B, Song J, Wang M, et al. BSA-bioinspired gold nanorods loaded with immunoadjuvant for the treatment of melanoma by combined photothermal therapy and immunotherapy. *Nanoscale*. 2018;10(46):21640–21647. doi:10.1039/c8nr05323e
24. Zhong J, Wen L, Yang S, et al. Imaging-guided high-efficient photoacoustic tumor therapy with targeting gold nanorods. *Nanomedicine*. 2015;11(6):1499–1509. doi:10.1016/j.nano.2015.04.002
25. Zhang X, Xi Z, Machuki JO, et al. Gold cube-in-cube based oxygen nanogenerator: a theranostic nanoplatform for modulating tumor microenvironment for precise chemo-phototherapy and multimodal imaging. *ACS Nano*. 2019;13(5):5306–5325. doi:10.1021/acsnano.8b09786
26. Yang J, Zhang R, Zhao H, et al. Bioinspired copper single-atom nanozyme as a superoxide dismutase-like antioxidant for sepsis treatment. *Exploration*. 2022;2(4):20210267. doi:10.1002/EXP.20210267
27. Ma L, Shen X, Zhou H, et al. Synthesis of Cu_3P nanocubes and their excellent electrocatalytic efficiency for the hydrogen evolution reaction in acidic solution. *RSC Adv*. 2016;6(12):9672–9677. doi:10.1039/C5RA24427G
28. Zhao Y, Pan H, Lou Y, et al. Plasmonic Cu2− x S nanocrystals: optical and structural properties of copper-deficient Copper(I) sulfides. *J Am Chem Soc*. 2009;131(12):4253–4261. doi:10.1021/ja805655b
29. Hessel CM, Pattani VP, Rasch M, et al. Copper selenide nanocrystals for photothermal therapy. *Nano Lett*. 2011;11(6):2560–2566. doi:10.1021/nl201400z
30. Li W, Zamani R, Rivera Gil P, et al. CuTe nanocrystals: shape and size control, plasmonic properties, and use as SERS probes and photothermal agents. *J Am Chem Soc*. 2013;135(19):7098–7101. doi:10.1021/ja401428e
31. Chen YC, Chen ZB, Hsu YK. Novel p-n heterojunction copper phosphide/cuprous oxide photocathode for solar hydrogen production. *J Colloid Interface Sci*. 2018;523:201–207. doi:10.1016/j.jcis.2018.03.103
32. Hou C, Chen Q, Wang C, et al. Self-supported cedarlike semimetallic Cu_3P nanoarrays as a 3D high-performance Janus electrode for both oxygen and hydrogen evolution under basic conditions. *ACS Appl Mater Interfaces*. 2016;8(35):23037–23048. doi:10.1021/acsami.6b06251
33. Manna G, Bose R, Pradhan N. Semiconducting and plasmonic copper phosphide platelets. *Angew Chem Int Ed Engl*. 2013;52(26):6762–6766. doi:10.1002/anie.201210277
34. Wang M, Rao J, Wang M, et al. Cancer photo-immunotherapy: from bench to bedside. *Theranostics*. 2021;11(5):2218–2231. doi:10.7150/thno.53056
35. Duan X, Chan C, Lin W. Nanoparticle-mediated immunogenic cell death enables and potentiates cancer immunotherapy. *Angew Chem Intl Ed Engl*. 2019;58(3):670–680. doi:10.1002/anie.201804882
36. Deng X, Shao Z, Zhao Y. Solutions to the drawbacks of photothermal and photodynamic cancer therapy. *Adv Sci*. 2021;8(3):2002504. doi:10.1002/advs.202002504
37. Xie Z, Fan T, An J, et al. Emerging combination strategies with phototherapy in cancer nanomedicine. *Chem Soc Rev*. 2020;49(22):8065–8087. doi:10.1039/D0CS00215A
38. Ma J, Zhang LQ, He ZX, et al. Autism candidate gene *DIP2A* regulates spine morphogenesis via acetylation of cortactin. *PLoS Biol*. 2019;17(10):e3000461. doi:10.1371/journal.pbio.3000461
39. Zhou B, Wu Q, Wang M, et al. Immunologically modified $MnFe_2O_4$ nanoparticles to synergize photothermal therapy and immunotherapy for cancer treatment. *Chem Eng J*. 2020;396:125239. doi:10.1016/j.cej.2020.125239
40. Liang L, Wen L, Weng Y, et al. Homologous-targeted and tumor microenvironment-activated hydroxyl radical nanogenerator for enhanced chemoimmunotherapy of non-small cell lung cancer. *Chem Eng J*. 2021;425:131451.
41. Ma Y, Xiao F, Lu C, et al. Multifunctional nanosystems powered photodynamic immunotherapy. *Front Pharmacol*. 2022;13:905078. doi:10.3389/fphar.2022.905078
42. Chen Y, Wang M, Zheng K, et al. Antimony nanopolyhedrons with tunable localized surface plasmon resonances for highly effective photoacoustic-imaging-guided synergistic photothermal/immunotherapy. *Adv Mater*. 2021;33(18):e2100039. doi:10.1002/adma.202100039
43. Zhou F, Yang J, Zhang Y, et al. Local phototherapy synergizes with immunoadjuvant for treatment of pancreatic cancer through induced immunogenic tumor vaccine. *Clin Cancer Res*. 2018;24(21):5335–5346. doi:10.1158/1078-0432.CCR-18-1126
44. Luo L, Yang J, Zhu C, et al. Sustained release of anti-PD-1 peptide for perdurable immunotherapy together with photothermal ablation against primary and distant tumors. *J Control Release*. 2018;278:87–99. doi:10.1016/j.jconrel.2018.04.002
45. Chen Q, Hu Q, Dukhovlinova E, et al. Photothermal therapy promotes tumor infiltration and antitumor activity of CAR T cells. *Adv Mater*. 2019;31(23):e1900192. doi:10.1002/adma.201900192
46. Lin X, Wang X, Li J, et al. Localized NIR-II photo-immunotherapy through the combination of photothermal ablation and in situ generated interleukin-12 cytokine for efficiently eliminating primary and abscopal tumors. *Nanoscale*. 2021;13(3):1745–1758. doi:10.1039/D0NR06182D
47. Yang Z, Gao D, Guo X, et al. Fighting immune cold and reprogramming immunosuppressive tumor microenvironment with red blood cell membrane-camouflaged nanobullets. *ACS Nano*. 2020;14(12):17442–17457. doi:10.1021/acsnano.0c07721
48. Munn DH, Mellor AL. IDO in the tumor microenvironment: inflammation, counter-regulation, and tolerance. *Trends Immunol*. 2016;37(3):193–207. doi:10.1016/j.it.2016.01.002
49. Uyttenhove C, Pilotte L, Theate I, et al. Evidence for a tumoral immune resistance mechanism based on tryptophan degradation by indoleamine 2,3-dioxygenase. *Nat Med*. 2003;9(10):1269–1274. doi:10.1038/nm934

50. Hwu P, Du MX, Lapointe R, et al. Indoleamine 2,3-dioxygenase production by human dendritic cells results in the inhibition of T cell proliferation. *J Immunol*. 2000;164(7):3596–3599. doi:10.4049/jimmunol.164.7.3596
51. Muller AJ, Manfredi MG, Zakharia Y, et al. Inhibiting IDO pathways to treat cancer: lessons from the ECHO-301 trial and beyond. *Semin immunopathol*. 2019;41:41–48. doi:10.1007/s00281-018-0702-0
52. Peng J, Xiao Y, Li W, et al. Photosensitizer micelles together with IDO inhibitor enhance cancer photothermal therapy and immunotherapy. *Adv Sci*. 2018;5(5):1700891. doi:10.1002/advs.201700891
53. Liu Y, Wu J, Jin Y, et al. Copper(I) Phosphide nanocrystals for in situ self-generation magnetic resonance imaging-guided photothermal-enhanced chemodynamic synergetic therapy resisting deep-seated tumor. *Adv Funct Mater*. 2019;29(50):1904678. doi:10.1002/adfm.201904678
54. Wang H, Shrestha TB, Basel MT, et al. Hexagonal magnetite nanoprisms: preparation, characterization and cellular uptake. *J Mater Chem B*. 2015;3(23):4647–4653. doi:10.1039/C5TB00340G
55. Liu J, Meyns M, Zhang T, et al. Triphenyl phosphite as the phosphorus source for the scalable and cost-effective production of transition metal phosphides. *Chem Mater*. 2018;30(5):1799–1807. doi:10.1021/acs.chemmater.8b00290
56. Zhou J, Wang G, Chen Y, et al. Immunogenic cell death in cancer therapy: present and emerging inducers. *J Cell Mol Med*. 2019;23(8):4854–4865. doi:10.1111/jcmm.14356
57. Krysko DV, Garg AD, Kaczmarek A, et al. Immunogenic cell death and DAMPs in cancer therapy. *Nat Rev Cancer*. 2012;12(12):860–875. doi:10.1038/nrc3380
58. Wang M, Song J, Zhou F, et al. NIR-triggered phototherapy and immunotherapy via an antigen-capturing nanoplatform for metastatic cancer treatment. *Adv Sci*. 2019;6(10):1802157. doi:10.1002/advs.201802157
59. Wculek SK, Cueto FJ, Mujal AM, et al. Dendritic cells in cancer immunology and immunotherapy. *Nat Rev Immunol*. 2020;20(1):7–24. doi:10.1038/s41577-019-0210-z
60. Dilioglou S, Cruse JM, Lewis RE. Function of CD80 and CD86 on monocyte-and stem cell-derived dendritic cells. *Exp Mol Pathol*. 2003;75 (3):217–227. doi:10.1016/S0014-4800(03)00072-8
61. Sun Y, Zhang Y, Gao Y, et al. Six birds with one stone: versatile nanoporphyrin for single-laser-triggered synergistic phototheranostics and robust immune activation. *Adv Mater*. 2020;32(48):e2004481. doi:10.1002/adma.202004481
62. Potula R, Poluektova L, Knipe B, et al. Inhibition of indoleamine 2,3-dioxygenase (IDO) enhances elimination of virus-infected macrophages in an animal model of HIV-1 encephalitis. *Blood*. 2005;106(7):2382–2390. doi:10.1182/blood-2005-04-1403